Solid Freeform Fabrication 2021: Proceedings of the 32nd Annual International Solid Freeform Fabrication Symposium – An Additive Manufacturing Conference
Reviewed Paper

Discrete Element Modeling of Fused Deposition Modeling Process

Menezes, C. and Turner, C.*

Department of Mechanical Engineering, Clemson University, Clemson, SC, USA 29631
* Contact Author (cturne9@clemson.edu)

Abstract

Fused Deposition Modeling components show anisotropic material properties as a result of the difference in bonding strengths between inter- and intra-layer particles. This difference occurs due to temperature gradient of the deposited filaments which affects the filament adhesion as well as due to the presence of voids or other discontinuities in the printed object. Discrete Element Modelling (DEM) is a discontinuous methodology which follows the idea of treating filaments as discrete rigid particles with simplified geometries for calculating the thermal interactions between the particles. Models using this approach allow the investigators to correlate the adhesion effects between filaments based on experimental data which ultimately will allow for optimization of the relevant printing parameters.

Introduction

Additive Manufacturing (AM) builds parts by sequentially adding material, often in the form of layers to an existing part, as opposed to the traditional practice of subtractive manufacturing where material is removed from a larger piece of material to leave a desired part. Multiple types of AM processes exist, including Stereolithography (SLA), Selective Laser Sintering (SLS), Fused Deposition Modelling (FDM), Inkjet Modeling (IJM), Direct Metal Deposition (DMD), and Layered Object Manufacturing (LOM). The differences in these techniques are largely defined by the mechanism by which new layers are created and by the materials usable in each technique [1].

While the initial machines were expensive and thus limited the technology to specialty customers [2], technology development has enabled these machines to move into increased use for prototyping and now for manufacturing. Consumer grade versions of many of these machines are already available and support a growing competitive home-market for AM products as well as a competitive sector of companies focused on "job-shop" AM services [3]. FDM is one of the easiest technologies to commercialize and is often an entry point for AM systems. FDM is primarily a polymer-based AM technique [2] that extrudes raw material in filaments through a heated extrusion nozzle as shown in Figure 1. Filaments are extruded in adjacent passes of the machine to form a layer, and subsequent layers are built one on top of another.

The quality and material properties of FDM parts are effected by various in-process parameters such as layer thickness, build orientation, print speed, extrusion temperature, infill density, and infill pattern [4], in addition to other parameters. Additives used to color or otherwise modify the filaments can decrease the quality and mechanical performance of FDM manufactured parts [5, 6] and environmental factors like humidity and temperature [6] can also affect the quality of the builds. Part quality is also dependent upon the accuracy and precision of the slicer software

that converts the CAD model to .STL file and the .STL file to g-code instructions which is the tool path followed by the nozzle. Machine parameters may further limit the quality of the build by the introduction of dynamic effects. The print time leads to different bonding behaviors when comparing the bonds within a single filament (intrafilament bonds), between filaments within a layer (intralayer bonds), and between layers (interlayer bonds). Cumulatively, these effects lead to FDM manufactured parts that may exhibit non-homogeneous, anisotropic and nonlinear behaviors [7], and to the products have quality control issues including dimensional errors, delamination between filaments and layers, undesirable porosity and poor or unpredicted material properties [8]. Yet, the ability to build simulations of the build process [3] that can lead to models that can accurately and reliably predict the material properties of the finished product in needed [9].

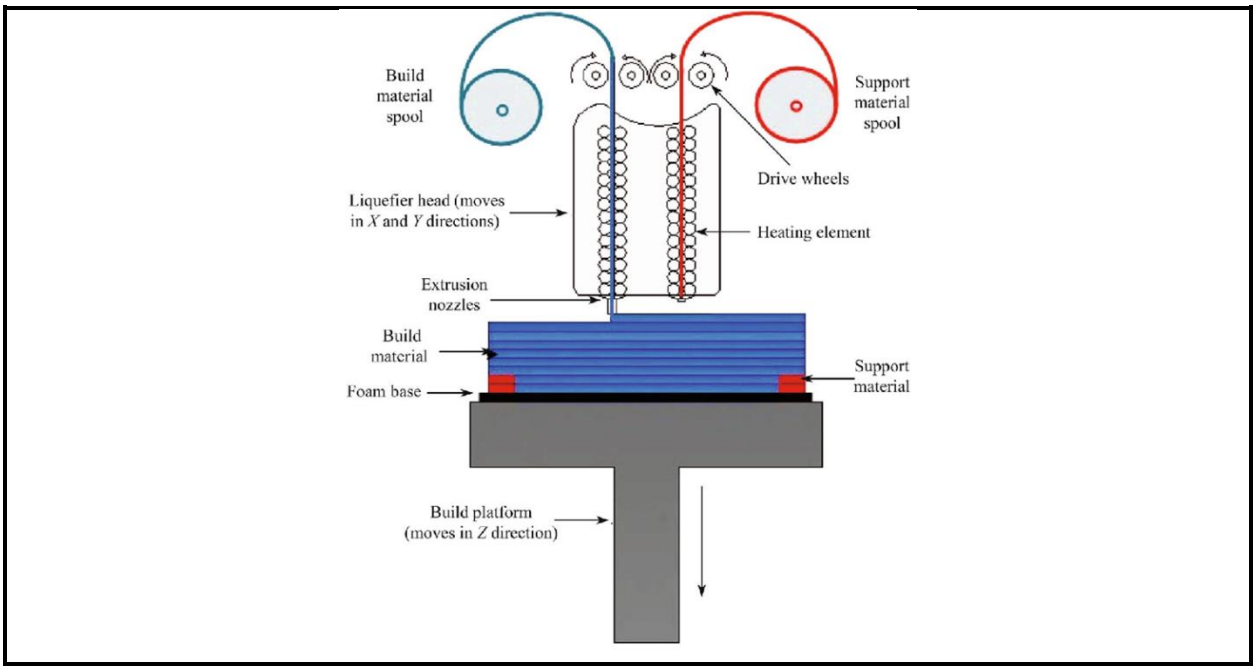

FIGURE 1: Schematic of the FDM Process, Adapted from [4].

Background

Following a path determined by the slicing software, FDM moves the extruder through the workspace depositing semi-molten material to form filaments. The bonds formed by the filament as it cools are primarily driven by the initial thermal energy of the semi-molten material at deposition [10] and the resulting polymer diffusion enabled by the filament temperature [11]. Cooling of the filament is controlled by heat transfer to the ambient environment (primarily through conduction and convection to the air, by conduction to adjacent materials in contact with the filament (i.e. other filaments and the build plate) [12]. The cooling profile of the filament as a function of its position and time is therefore an important factor in the resulting mechanical properties of the printed part.

Prior research has considered this problem through the use of finite difference methods [13, 14] and finite elemental analysis [15-17]. These methods assume that the part is a continuum. Other researchers, [12, 18, 19] have been developed analytical solutions where the transient heat model includes activating or deactivating all relevant local boundary conditions depending on part

geometry, operating conditions and deposition strategy. A related mathematical approach treats the filament as discrete particles (or elements) and can be used to construct systems with various boundary conditions to simulate thermal and mechanical changes between elements [20]. This discrete element method (DEM) approach is particularly popular when simulating powder-based AM techniques such as SLS [21]. Our focus is in developing these methods as a means to simulate the behavior of an FDM process by representing the filament as a sequence of discrete particle elements.

Methodology

In a typical DEM approach, a discrete element of spherical shape is used to represent an element. A spherical shape is used because it simplifies the contact calculations with adjacent elements. However, when simulating a filament, the initial spherical shape quickly "slumps" to form a filament with an oblong cross-section. While a higher fidelity element model could be used to account for this mechanical slumping behavior, we chose in our initial model to simply assume that the element remains round and will have a diameter equal to the layer height of the printed part. Consequently, the filament width is equal to the layer height. Note that this assumption may prove to be inaccurate, but for an initial model, we feel that it is a reasonable first approximation of the behavior of the filament.

Furthermore, for our initial model, we decoupled the g-code process from the model creation process and focused on the development of rectangular parts with a solid infill pattern composed of filaments deposited as shown in Figure 2. Since for most FDM printers, the layer height values range from (0.2 mm to 0.4mm), the resulting Biot number (Bi), is less than 0.1. Hence, each element can be considered to be a lumped capacity element which assumes uniform temperature distribution across the cross-sectional element area. Thus, each layer is composed of a single filament (18 elements long in Figure 2) laid down in a zig-zag pattern. As is typical of slicing programs, subsequent layers are often formed with a zig-zag patten orthogonal to the layer below. We adopted this approach to simplify the initial program and will integrate a g-code based path planning algorithm in future versions of the code.

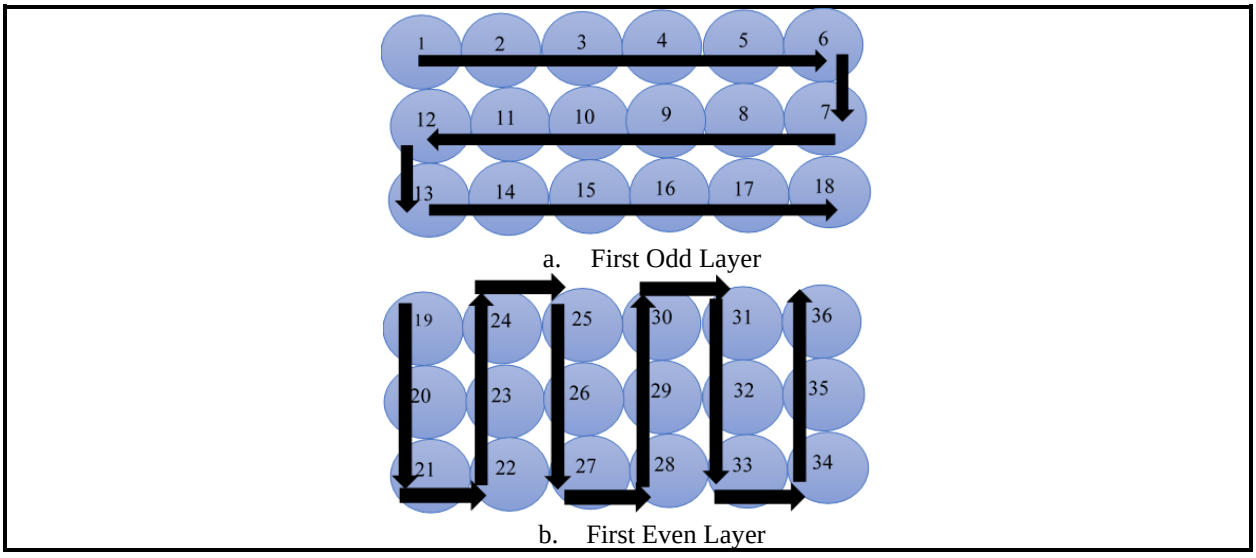

Figure 2: Modeled Deposition Sequence.

Based on these assumptions, we can define some of the mathematical properties of the elements. The surface area of the element is that of a sphere with a radius, R.

$$A = 4\pi R^2 \tag{1}$$

Similarly, the element has a volume of a sphere of radius, R.

$$V = \frac{4}{3}\pi R^3 \tag{2}$$

Since the thermal energy stored in an element is a function of the volume, density, heat capacity and the temperature of the element we can write

$$U_{deposition} = \rho V C_p \left(T_{deposition} - T_{amb}\right) \tag{3}$$

Here, we make another assumption, that the resulting element has "good" contact with any adjacent elements such that the area in contact is given by

$$A_{contact} = \frac{A}{6} \tag{4}$$

While a true rigid sphere would have only point contact with its neighbor, this contact approximation is that of a cube in contact with other cubes. Since in reality our sphere is not rigid, but is in fact "mushy", this assumption is probably closer to the reality, although it is not also imperfect. Thus, by applying Fourier's Law, we can find that the conductive heat transfer is

$$\dot{Q}_C = \frac{\left(T_A - T_B\right)}{R_{th}} \tag{5}$$

where the thermal resistance R_{th} is

$$R_{th} = \frac{L}{kA_{contact}} \tag{6}$$

where L is the characteristic length, and k is the material conductivity. For this model, the characteristic length is given by

$$L = \frac{V}{A_{contact}} = \frac{R}{3} \tag{7}$$

We can apply similar techniques to model convection and radiation effects on each of the six faces of the element. Initially, we will assume that only free convection is present, and that radiative heat transfer is negligible. Thus, we can determine that the internal energy, U_i, of the element at a time t_i, is given by:

$$U_i = U_{i-1} - \dot{Q}_{conduction}\Delta t - \dot{Q}_{convection}\Delta t \qquad (8)$$
$$and \quad \Delta t = t_i - t_{i-1}$$

and so, the temperature T_i, of the element is given by rearranging Equation (3) as

$$T_i = \frac{U_i}{\rho C_p V} + T_{amb} \qquad (9)$$

where we assume that the deposition time, t_i, of the element is at i = 0. At deposition, the temperature of the element is that of the extruder, which we refer to as the deposition temperature.

Based on this formulation, we can have several different heat transfer boundary conditions that need to be modeled. The first element deposited (element 1 in Figure 2) has five faces exposed to the ambient environment, where conduction to the ambient atmosphere and free convection are the modes of heat transfer. These conditions apply to the left, right, front, back and top faces of the element. However, the bottom face is in "good" contact with the build plate and in this case only experiences a conductive heat transfer to the build plate. If the build plate is cooler than the element, heat flows from the element into the build plate, cooling the element, and if the build plate is warmer than the element, heat flows from the build plate into the element, further warming the element.

When the second element is deposited next to element 1 (on the right side of element 1) in Figure 2, the right hand side of element 1 changes its boundary conditions. Element 1 no longer has a free convection mode on its right face, and its conduction mode changes from the ambient atmosphere to a conduction mode with element 2. The other faces remain in the same heat transfer states. Element 2 begins with free convection and atmospheric conduction on four faces, right, front, back and top, but experiences conduction with element 1 on its left face, and conduction with the build plate on its bottom face.

Ultimately, there are 12 heat transfer cases that need to be considered. Six of the cases involve the build plate and various numbers of faces exposed to the atmosphere or to other elements. The remaining 6 cases involve situations where some faces are in contact with other elements and some faces are in contact with the ambient atmosphere. The model determines the appropriate boundary case for each element based on the flowchart presented in Figure 3.

The model was initially formulated in MatLAB™ to evaluate our results against several test cases to determine if the initial assumptions appear to be valid. This formulation would also allow us to use the model to compare to previous experimental data sets generated by [9]. However, due to the larger size of these data sets, use of the campus Palmetto cluster would be necessary. Fortunately, with the model formulated in MatLAB™, the process of running the model on the cluster did not require substantial modifications to the existing code.

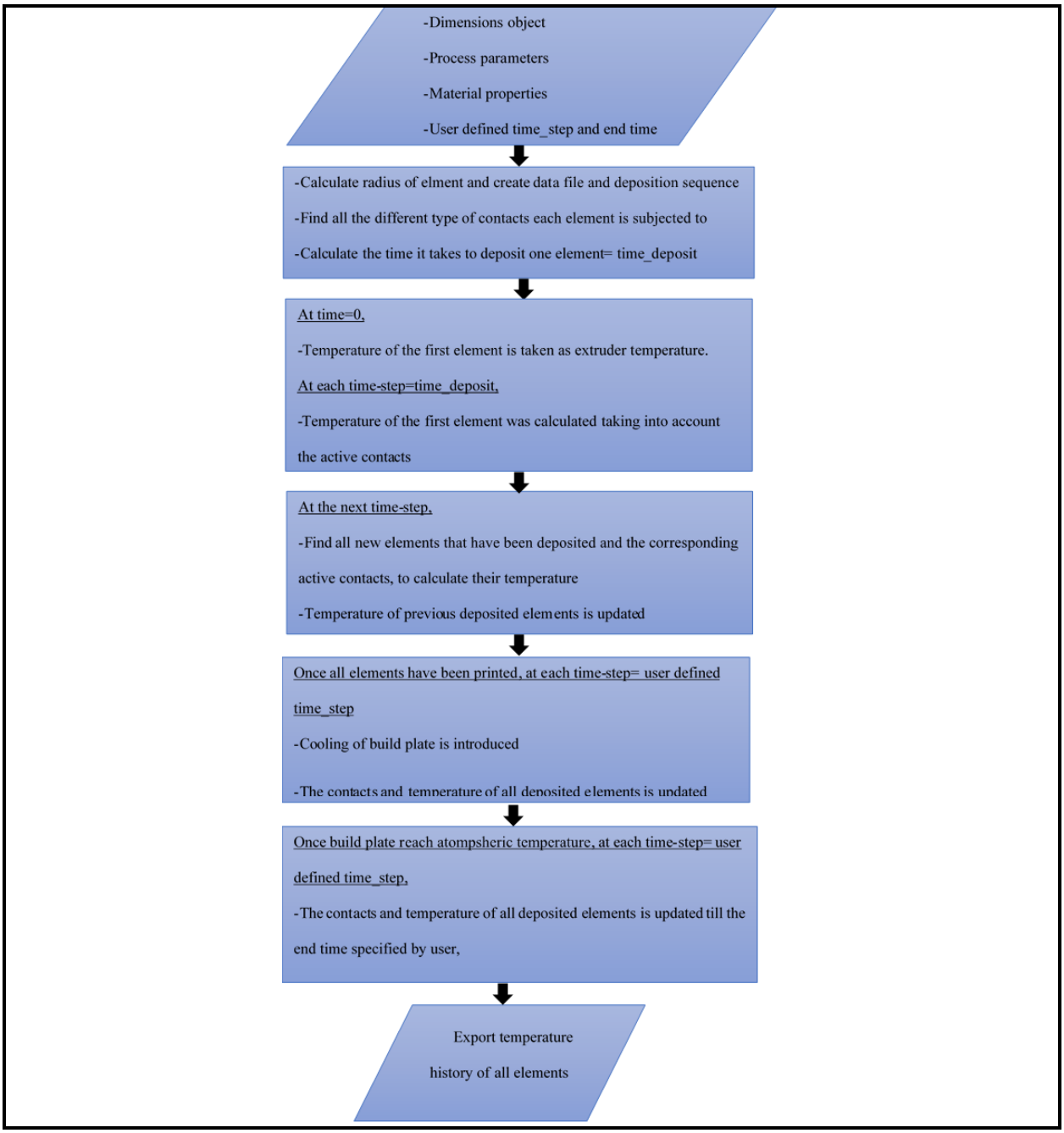

FIGURE 3: Model Flow Chart.

Preliminary Validation Tests

For this work, we will present the results for three test cases representing specimens of different sizes. The process parameters and materials properties for the tests are shown in Table 1. The parameters of the three test cases are shown in Table 2.

Table 1. Process parameters and material properties

Property	Value
Velocity of extruder (m/s)	0.05
Layer height (m)	0.0004
Extruder temperature (K)	493
Ambient (Atmospheric) temperature (K)	298
Specific heat capacity of PLA (J/kg·K)	1800
Density of PLA filament (kg/m^3)	1240
Built plate temperature (K)	333
Rate of cooling of build plate (K/s)	0.08334
Thermal conductivity of PLA (W/m·K)	0.13
Thermal conductivity of Build plate Glass (W/m·K)	0.8

Table 2. Test cases

	Layers	Rows	Columns	Total Elements	Size of printed part (LxWxH) (mm)
Dataset 1	6	25	10	1500	(4x10x2.4)
Dataset 2	6	16	16	1536	(6.4x6.4x2.4)
Dataset 3	10	10	25	2500	(10x4x4)

The first two trials represent a rectangular and a square specimen, each with six layers. Odd layers are thus printed in a horizontal direction while even layers are printed in a vertical direction. The third data set is also rectangular but printed in a 90 degree orientation to that of dataset 1, and comprises ten layers instead of six. Again, odd layers are printed horizontally, and even layers are printed vertically. For each test case, we recorded the temperature histories for each element. Figure 4 shows the temperature history for all three datasets at the midpoint of the printing process. For dataset 1 that would be after the 750th element, for dataset 2 the 768th element, and for dataset 3 after the 1250th element. Elements not yet printed show a printing temperature of 0 Kelvin in Figure 4.

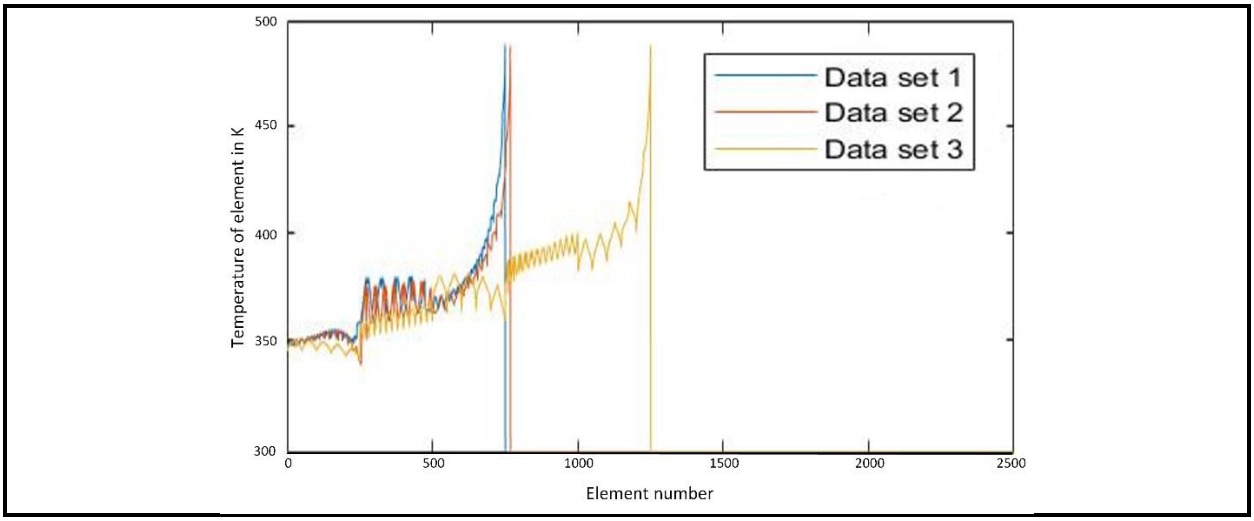

FIGURE 4: Element temperatures at printing midpoint.

Note in Figure 4 that the most recent element is also the element at the highest temperature and that the elements are generally cooler the longer it has been since the element was first deposited. It is also apparent that the cooling rate is not uniform, and in fact we see some variation of the temperature of the elements with the elements on the edges of the specimen cooling faster than those internal to the specimen. This phenomenon is more extreme when the printing direction is a shorter length as is the case with the odd layers in dataset 3 and the even layers of dataset 1 (where the filament length is each 10 elements) compared to the longer 16 element lengths in dataset 2 and the 25 element lengths in datasets 1 and 3. This makes physical sense in that the external elements are better able to expel heat than the internal elements.

If we examine the same data once the entire part has been printed, as shown in Figure 5, we see the same trends are also apparent. Notice that the elements in the part now have temperatures ranging from about 340K to the extruder temperature of 493K.

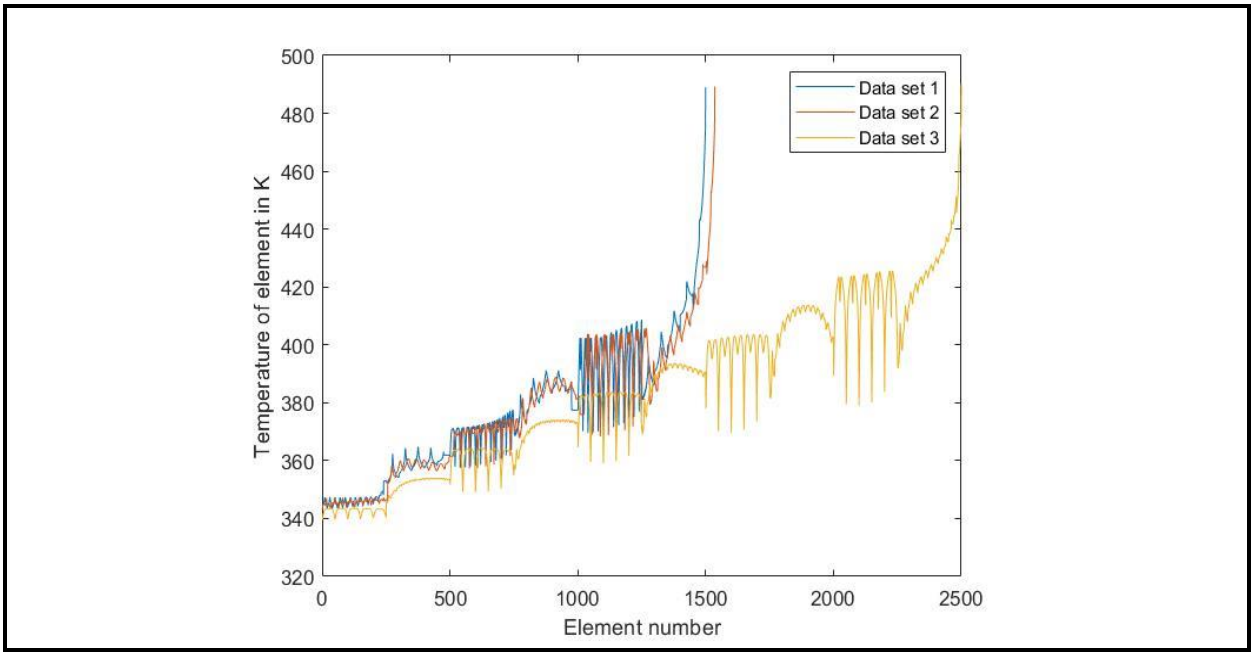

FIGURE 5: Element temperatures at printing endpoint.

Once the print is complete, we begin a process of allowing the build plate to cool from a heated temperature of 333K to a plate temperature 298K over several minutes. We continue to monitor the temperatures of the elements awaiting the part to cool to ambient temperature. Figure 6 shows the temperature profiles a quarter of the time through this cooling process. Note that the cooling pattern has inverted itself, and the elements farthest from the build plate are now the coolest elements in the model. Similarly, the span of temperature of the part is now less than 3K as opposed to the 160K when the build was complete. And while the edge elements are slightly cooler than the interior, the temperature gradient between the interior and edges is far less significant than it was earlier in the simulation.

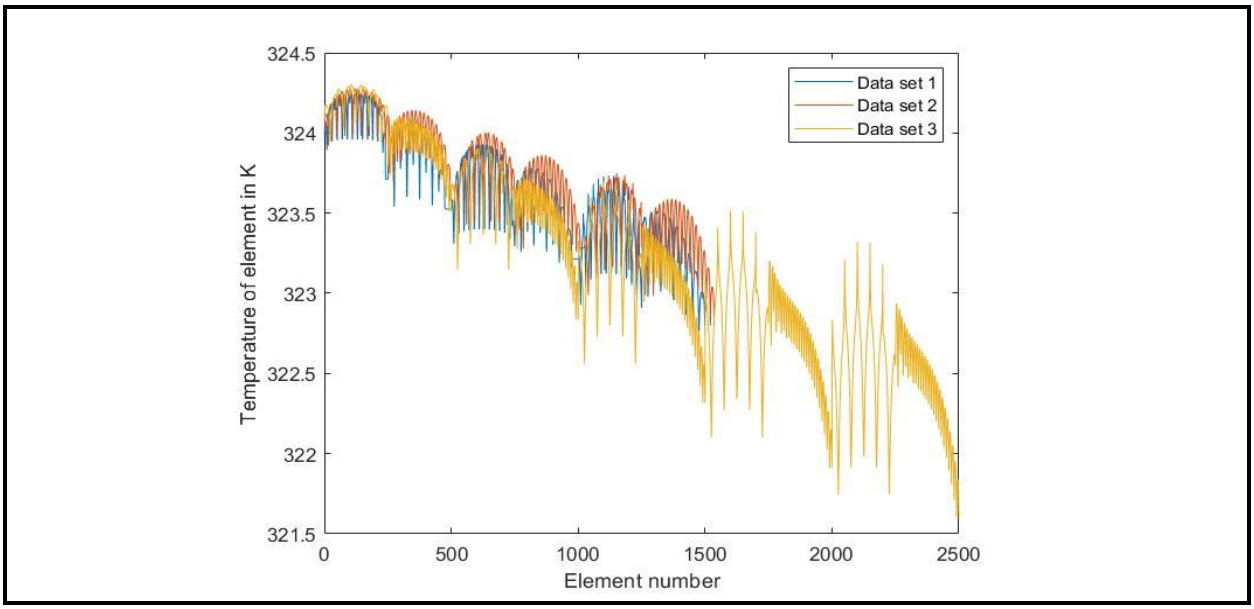

FIGURE 6: Element temperatures at a quarter of the time through the cooling process.

In Figure 7, the temperature profiles of the elements at the midpoint of the plate cooling process continue to show a similar trend. Except now the range of temperatures is about 1.5K.

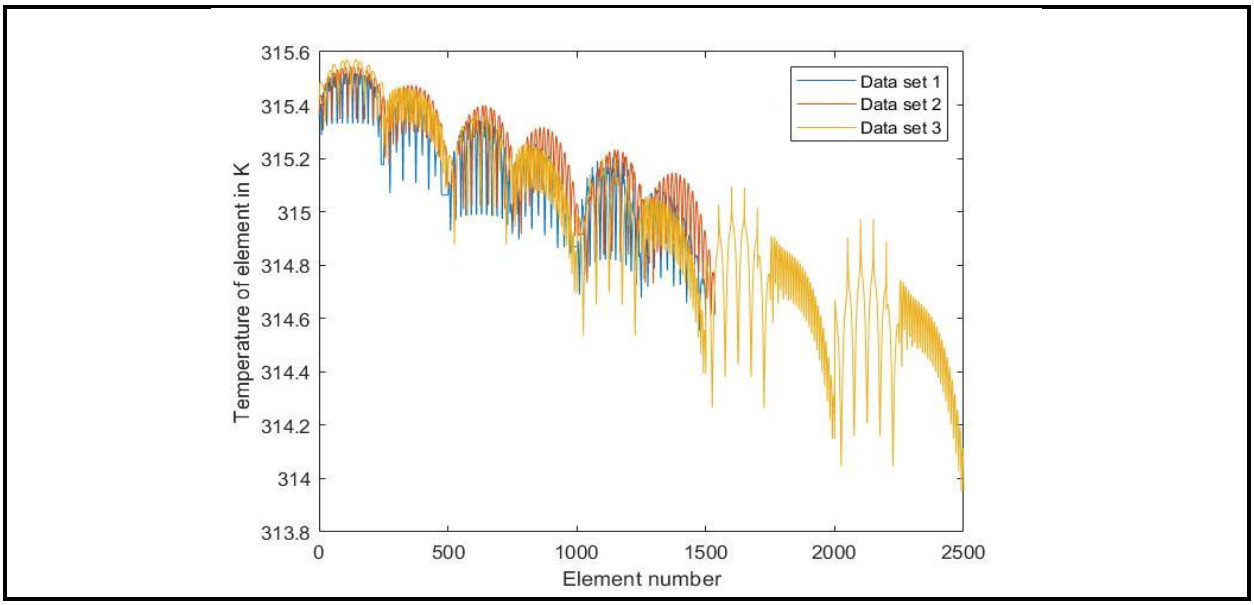

FIGURE 7: Element temperatures at half of the time through the cooling process.

While Figure 8 initially appears to show that the temperature gradient within he part is increasing, by examining the temperature axis, it can bee seen that the range of variation is now approximately 0.5K, indicating that the part is continuing to approach an isothermal state.

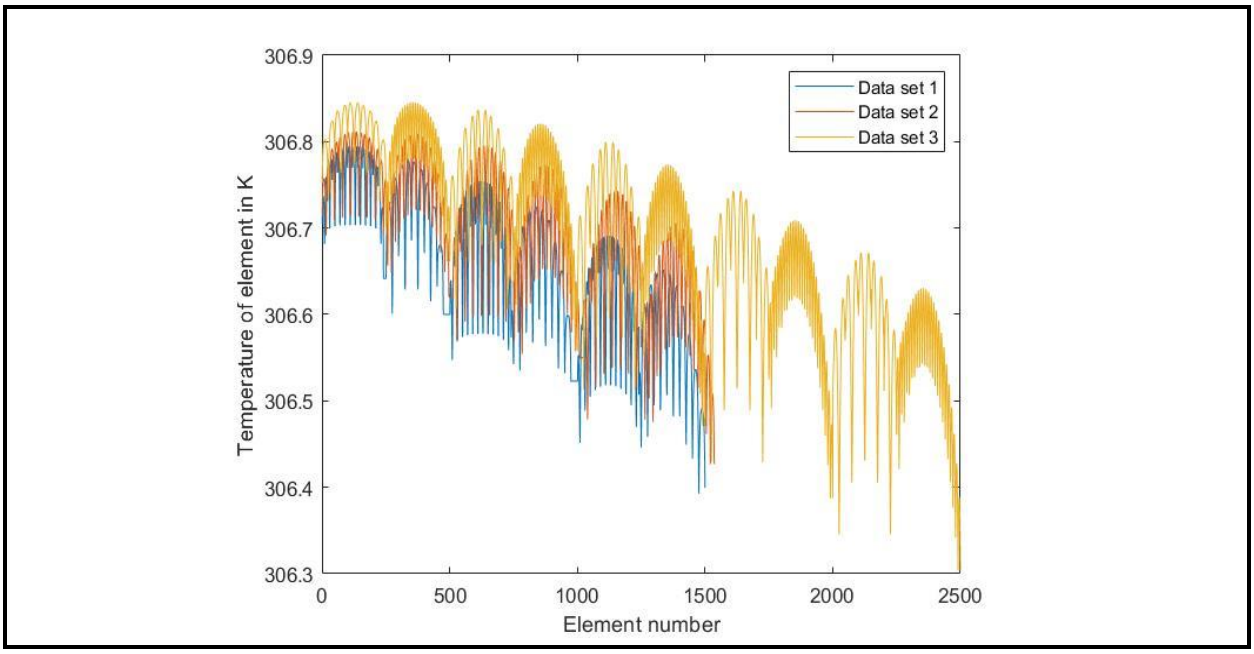

FIGURE 8: Element temperatures at three-fourths of the time through the cooling process.

Finally, in Figure 9, we observe that the part has effectively cooled to the build plate temperature of 298K, with a temperature variation of approximately 0.5K throughout the part.

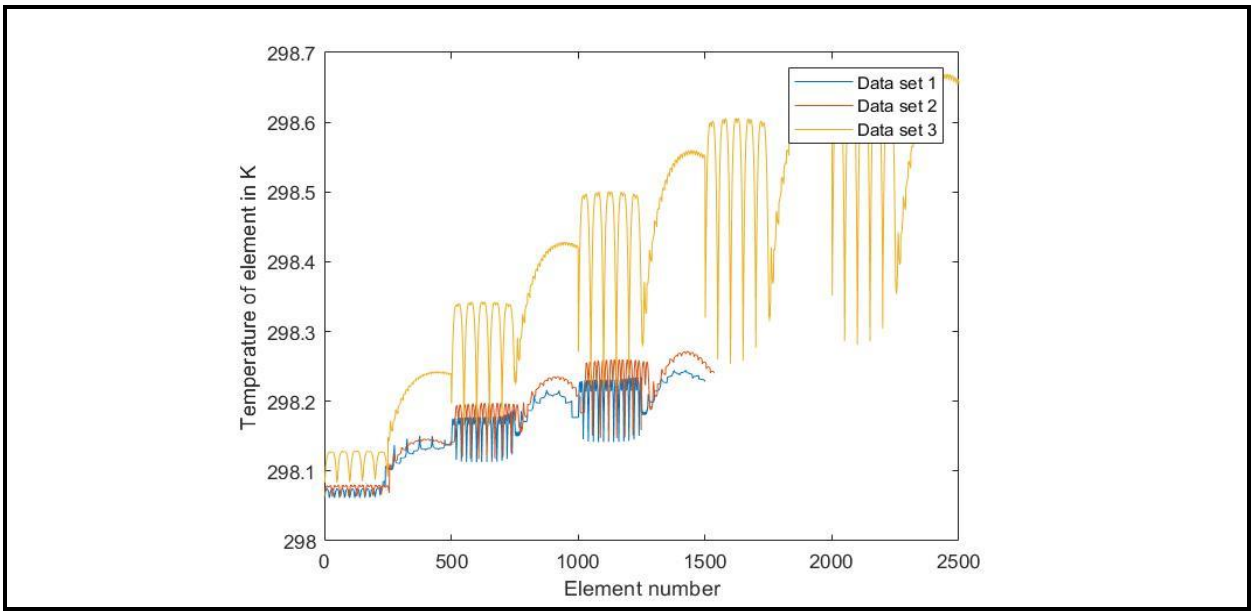

FIGURE 9: Element temperatures at the end of the simulation.

These behaviors appear to mimic observed physical processes, where the part cools from the outside-to-the-inside, and where heating the build plate prolongs the time that the layers closest to the build plate build polymer connections between filaments (intralayer) and between layers (interlayer). This further explains the anisotropic behaviors observed, where the layers adjacent to the build plate approximate bulk material properties, while the layers furthest removed from the build plate demonstrate increased anisotropic behaviors related to the filament orientations.

Conclusions and Future Work

These trials demonstrate that the DEM simulation constructed appears to mimic the thermal behavior of cooling FDM materials despite the simplifying assumptions made to construct the DEM model. Encouragingly, we even observed cooling differences due to the proximity to the edges of the build and due to the warming effects of a heated build plate. We believe that qualitatively, the model is matching observed behaviors.

However, quantitative evaluation of the model remains incomplete. We will need to evaluate the observed cooling rates versus experimental data to confirm that the predicted cooling temperatures are valid. In addition, the incorporation of a g-code based scheme to match a generically sliced model is necessary to compare to the much wider range of print configurations available in actual AM processes. Furthermore, there are several opportunities to improve the computational performance of the model.

Our initial goal is to analyze the thermal behavior of elements in the model to predict the time during which adjacent elements are at a suitable temperature to form bonds between the elements. This relationship should demonstrate that there are bond formation time differences between intrafilament, intralayer and interlayer bonds that correspond to observed differences in material modulus in these directions [9]. This analysis should assist in determining whether a simple thermal model is adequate, or whether a more complex mode incorporating surface effects is necessary to predict these bond strengths within a desired range of accuracy.

Additional effects, such as the mechanical "slump" experienced by the filament upon deposition (attributable to the viscosity of the material) and as a result of the weight of additional layers added on top of the initial layers of filament should allow for the model to also account for dimensional effects furing printing, and potentially even curling effects. Understanding these effects in simulation may allow for advanced build plates that allow for regionalized heating and cooling of the part during the build process to optimize dimensional stability and promote bonding. Furthermore, future DEM models can use the build information to account for induced stresses and to predict part strengths and anisotropic properties by incorporating additional models of multiphysics effects. This capability would allow a part to be optimized with the design-build-and-use cases fully considered before the part is ever printed, supporting process certification.

The initial model described in this work is but a first step towards a full multiphysics model that can examine a host of potential improvements to the FDM process. Furthermore, the insights gained in developing this model can be applied to models of other AM processes leading to a fuller picture of the complex multiphysics effects present in AM processes. Understanding, predicting, and using these effects is entirely within the realm of possibilities for computationally supported AM models as a result of this work and work like this. We are pleased with our initial results and encourage work to continue in this and other avenues to support a multiphysics understanding of additive manufacturing from design, through the build process, to the end use of the parts.

Acknowledgements

The authors would like to acknowledge the support of the Department of Mechanical Engineering at Clemson University for their support of this work. All statements within are those of the authors and may or may not represent the views of these institutions.

References

[1] Pereira, T., Kennedy, J. V., and Potgieter, J., 2019, "A Comparison of Traditional Manufacturing Vs Additive Manufacturing, the Best Method for the Job," Procedia Manufacturing, **30** pp. 11-18.
[2] Rafiq, N., 2006, " Rapid prototyping : principles and applications," Wiley, Hoboken, N.J.
[3] Migler, K., and Ricker, R., 2016, "Measurement Science Roadmap for Polymer-Based Additive Manufacturing," Advanced Manufacturing Series, NIST ADM, https://doi.org/10.6028/NIST.AMS.100-5 .
[4] Dey, A., and Yodo, N., 2019, "A Systematic Survey of FDM Process Parameter Optimization and their Influence on Part Characteristics," Journal of Manufacturing and Materials Processing, **3** pp. 64.
[5] Pandžić, A., Hodzic, D., and Milovanović, A., 2019, "Influence of Material Colour on Mechanical Properties of PLA Material in FDM Technology ," .
[6] Valerga, A. P., Batista, M., Salguero, J., 2018, "Influence of PLA Filament Conditions on Characteristics of FDM Parts," Materials (Basel, Switzerland), **11**(8) pp. 1322.
[7] Ahn, S., Montero, M., Odell, D., 2002, "Anisotropic Material Properties of Fused Deposition Modeling ABS," Rapid Prototyping Journal, **8** pp. 248-257.
[8] Sood, A. K., Ohdar, R., and Mahapatra, S., 2009, "Improving Dimensional Accuracy of Fused Deposition Modelling Processed Part using Grey Taguchi Method," Materials & Design, **30** pp. 4243-4252.
[9] Baikerikar, P. and Turner, C. 2021, "Comparison of FEA simulations and experimental results for as-built additively manufactured dogbone specimens," International Journal of Advanced Manufacturing Technology, https://doi.org/10.1007/s00170-021-07307-9.
[10] Sun, Q., Rizvi, G., Bellehumeur, C. T., 2003, "Experimental Study of the Cooling Characteristics of Polymer Filaments in FDM and Impact on the Mesostructures and Properties of Prototypes," Solid Free.Fabr.Proc., Austin, Texas, pp. 313-323.
[11] Coogan, T. J., and Kazmer, D. O., 2017, "Healing Simulation for Bond Strength Prediction of FDM," Rapid Prototyping Journal, 23(3) pp. 551-561.
[12] Costa, Duarte, F., and Covas, J., 2015, "Thermal Conditions Affecting Heat Transfer in FDM/FFE: A Contribution Towards the Numerical Modelling of the Process," Virtual and Physical Prototyping, 10.
[13] Zhang, J., Wang, X. Z., Yu, W. W., 2017, "Numerical Investigation of the Influence of Process Conditions on the Temperature Variation in Fused Deposition Modeling," Materials and Design, pp. 59-68.
[14] Stockman, T., Schneider, J., Walker, B., 2019, "A 3D Finite Difference Thermal Model Tailored for Additive Manufacturing," Jom, 71.
[15] Ji, L., and Zhou, T., 2010, "Finite Element Simulation of Temperature Field in Fused Deposition Modeling," Advanced Materials Research, 97-101 pp. 2585.
[16] D'Amico, A., and Peterson, A. M., 2018, "An Adaptable FEA Simulation of Material Extrusion Additive Manufacturing Heat Transfer in 3D," Additive Manufacturing, 21 pp. 422-430.
[17] Zhou, Y., Lu, H., Wang, G., 2020, "Voxelization Modelling Based Finite Element Simulation and Process Parameter Optimization for Fused Filament Fabrication," Materials & Design, 187 pp. 108409.
[18] Costa, S., Duarte, F., and Covas, J., 2017, "Estimation of Filament Temperature and Adhesion Development in Fused Deposition Techniques," Journal of Materials Processing Technology, 245 pp. 167-179.
[19] Costa, S., Duarte, F., and Covas, J., 2008, "Towards Modelling of Free Form Extrusion: Analytical Solution of Transient Heat Transfer," International Journal of Material Forming, 1 pp. 703-706.
[20] Wriggers, P., and Avci, B., 2020, "Modeling in Engineering using Innovative Numerical Methods for Solids and Fluids,"Springer International Publishing, Cham, pp. 1-30.
[21] Haeri, S., Wang, Y., Ghita, O., 2017, "Discrete Element Simulation and Experimental Study of Powder Spreading Process in Additive Manufacturing," Powder Technology, 306 pp. 45-54.